Materials Science and Engineering A 386 (2004) 20–26

www.elsevier.com/locate/msea

The role of solute titanium and TiB_2 particles in the liquid–solid phase transformation of aluminum alloys

N. Iqbal[a,*], N.H. van Dijk[a], T. Hansen[b], L. Katgerman[c], G.J. Kearley[a]

[a] *Interfaculty Reactor Institute, Delft University of Technology, Mekelweg 15, 2629 JB Delft, The Netherlands*
[b] *ILL, 6 Rue Jules Horowitz, BP 156, 38042 Grenoble Cedex 9, France*
[c] *Laboratory for Materials Science, Delft University of Technology, Rotterdamseweg 137, 2628 AL Delft, The Netherlands*

Received 27 January 2004; received in revised form 25 June 2004

Abstract

The nucleation and growth kinetics of α-Al grains in the systems Al–0.1Ti and Al–0.15TiB_2 (wt.%) have been studied by time-resolved neutron diffraction measurements during the liquid–solid phase transformation under continuous cooling. The evolution of the static structure factor $S(Q)$ was monitored for different cooling rates. The evolution of the solid fraction f_S for both samples during the transformation was determined from the normalized variation of the height of first peak in the liquid structure factor. The transformation kinetics was analyzed in terms of the Johnson–Mehl–Avrami model, and compared for both samples. The evolution of Bragg peaks emerging after the nucleation of the solid phase was monitored. The results reveal that the TiB_2 particles in pure aluminum are not effective nucleation sites for α-Al grains during solidification. However, the presence of solute titanium in the Al–0.1Ti alloy changes the growth rate of crystallization during solidification. In the early stages of the phase transformation in the Al–0.1Ti alloy, pronounced oscillations in the Bragg peaks intensity are observed. These observations are discussed in the light of the present grain refinement theories.

Keywords: Solidification; Aluminum alloys; Neutron diffraction; TiB_2; Structure factor

1. Introduction

The liquid to solid phase transformation has a vital influence on the macroscopic properties of aluminum alloys. A significant improvement of the mechanical properties of aluminum can be obtained by the addition of small amounts of Al–Ti–B master alloys [1,2]. These alloys contain microscopic TiB_2 and $TiAl_3$ nucleating particles. Experiences indicate that the Al–Ti–B alloys are effective grain refiners but similar alloys containing only TiB_2 or $TiAl_3$ particles are much less effective. Various theories regarding the grain refining mechanisms of Al–Ti–B refiners are proposed [3–8], such as the particle theory, the phase diagram theory, the duplex nucleation theory and the peritectic hulk theory. Although the idea that TiB_2 particles combined with solute titanium play a central role in the transformation process seems to be gaining wider acceptance [2,8], a complete understanding and general consensus of the mechanism(s) involved is still lacking. In order to obtain a better understanding of the grain refining mechanism(s) it is necessary to study the evolution of the liquid to solid phase transformation kinetics of these aluminum alloys, in situ, containing TiB_2 nucleant particles and solute Ti, separately and in combination.

We have previously reported the transformation kinetics of the liquid to solid phase transformation in pure aluminum and in a Al–0.3Ti–0.02B (wt.%) alloy containing both TiB_2 nucleant particles and solute Ti [9]. In the present paper the transformation kinetics and the effectiveness for grain refinement of both TiB_2 particles and of solute titanium in aluminum is studied separately, by time-dependent neutron diffraction measurements during the solidification of Al–0.15TiB_2 (wt.%) and Al–0.1Ti (wt.%) alloys for different continuous cooling rates. A big advantage of neutrons is that

* Corresponding author. Tel.: +31 15 278 4533; fax: +31 15 278 8303.
E-mail address: iqbal@iri.tudelft.nl (N. Iqbal).

0921-5093/$ – see front matter © 2004 Elsevier B.V. All rights reserved.
doi:10.1016/j.msea.2004.06.068

the bulk sample can be studied in situ, because of the large penetration length for neutrons into the sample.

2. Materials and method

2.1. Sample preparation

The studied samples were laboratory prepared from high purity aluminum, titanium and TiB_2 particles. The pure aluminum (99.999%) and titanium (99.99%) were purchased from Goodfellows. The TiB_2 (99.99%) powder with a particle size distribution ranging from 3 to 6 μm with a maximum around 4.4 μm was purchased from Advanced Ceramics.

The Al–0.15TiB_2 sample was prepared by putting aluminum lumps with a total mass of 35 g together with TiB_2 particles into an aluminum oxide crucible. The sample was heated to T = 1023 K. After holding at this temperature for 30 min, the crucible was removed from the furnace and the liquid alloy was homogenized by stirring using an aluminum oxide rod. After solidification the sample was remelted and the above mentioned process was repeated three times to ensure that the TiB_2 particles were homogeneously distributed in the Al–0.15TiB_2 sample. The solid sample was then cut into cylinders with a diameter of 9 mm.

In order to prepare the Al-0.1Ti sample, a different route was adopted. First, Al–1Ti master alloy samples, 5 g each, were prepared by melting together the appropriate amounts of aluminum and titanium in an electric arc furnace in a high purity argon atmosphere. The molten samples were stirred by using the arc flame for homogenization. Then the samples were solidified, rotated by changing the top and bottom positions, and remelted. This process was repeated five times to ensure that titanium is homogeneously distributed in the sample. Having prepared the Al–1Ti master alloy samples, the Al–0.1Ti sample was prepared by melting it together with an appropriate amount of high purity aluminum, by the method described for the Al–0.15TiB_2 sample.

Differential thermal analysis (DTA) measurements were performed on these samples, with sample dimensions 2 mm × 2 mm × 2 mm, to gain an estimate of the transition temperatures. The results revealed that for the slow cooling rate of 0.5 K/min, the liquid to solid transformation starts at T_s = 932.1 K, and the transformation is complete at T_f = 929.1 K for the Al–0.15TiB_2 alloy. For the Al–0.1Ti alloy, the transformation starts at T_s = 933.6 K, and the transformation is completed at T_f = 929.2 K for the cooling rate of 0.5 K/min.

2.2. Experimental method

In situ neutron diffraction measurements were performed at the high-flux powder diffractometer D20 at the Institute Laue-Langevin (ILL). Al–0.15TiB_2 and Al–0.1Ti alloy samples with a mass of 10 g were placed in a cylindrical single-crystalline sapphire container with a height of 60 mm, an inner diameter of 10 mm, and a wall thickness of 1 mm. A monochromatic neutron beam with wavelength of 0.94 Å and a beam height of 41 mm was used in all neutron diffraction experiments. For the high temperature neutron diffraction measurements a dedicated vacuum furnace (4×10^{-5} mbar) was used with a vanadium heater element and a temperature stability of about 1 K. In order to achieve the temperature stability required for our solidification experiments ($\Delta T < 50$ mK), a specially designed furnace insert was used [9].

3. Results and discussion

3.1. Liquid structure factor

In Fig. 1 the measured liquid structure factor, $S(Q)$, as a function of the wave-vector transfer, Q, is shown for the Al–0.15TiB_2 and Al–0.1Ti alloy samples at a temperature of T = 943 K. The observed structure factor is in agreement with previous neutron [9–11] and X-ray diffraction [12,13] studies of liquid aluminum in the vicinity of the solidification temperature. The first liquid peak for both samples is observed at $Q = 2.68$ Å^{-1} with a height of $S(Q)$ = 2.39 for the liquid Al–0.15TiB_2 alloy and $S(Q)$ = 2.56 for the liquid Al–0.1Ti, respectively. The previously studied samples of pure aluminum and Al–0.3Ti–0.02B alloy show a height of the first liquid peak at $Q = 2.68$ Å^{-1} of $S(Q)$ = 2.44 and 2.39, respectively. The measured structure factor of the liquid Al–0.15TiB_2 and Al–0.1Ti alloys closely resembles the curve of pure aluminum [9] indicating a weak influence of the alloying elements on the short-range order in the liquid.

3.2. Liquid volume fraction

In order to study the influence of TiB_2 particles and solute titanium on the crystallization behavior of aluminum, systematic time-dependent neutron diffraction measurements of the structure factor in Al–0.15TiB_2 and Al–0.1Ti alloys were per-

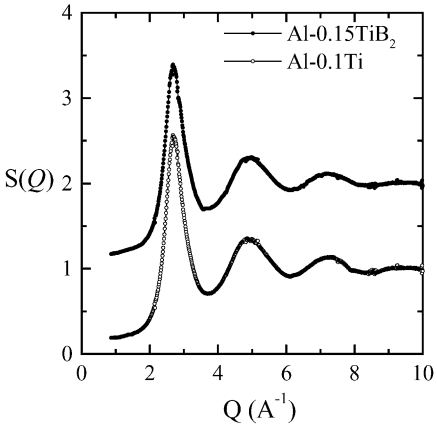

Fig. 1. Liquid structure factor $S(Q)$ as a function of the wave-vector transfer Q for the Al–0.15TiB_2 (solid circles) and the Al–0.1Ti alloy (open circles) at a temperature of T = 943 K. For clarity $S(Q)$ of the Al–1Ti alloy is vertically displaced by 1.

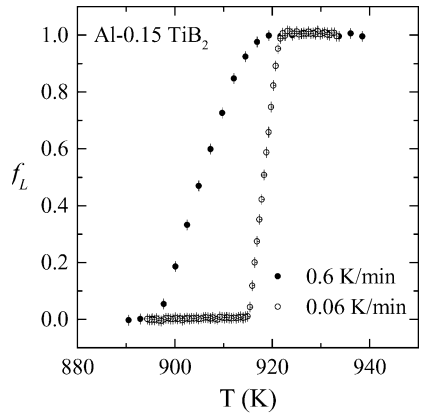

Fig. 2. Liquid volume fraction f_L of the Al–0.15TiB_2 alloy as a function of temperature for cooling rates of 0.06 K/min (open circles) and 0.6 K/min (solid circles). The liquid volume fraction f_L is deduced from the normalized variation in the first liquid peak in $S(Q)$ at $Q = 2.68$ Å^{-1}.

formed during solidification. For each of the measurements the sample was heated to a temperature of 943 K for 1 h to obtain a homogeneous liquid phase, followed by a continuous cooling with rates of 0.06 and 0.6 K/min for the Al–0.15TiB_2 alloy and 0.06, 0.2 and 0.6 K/min for the Al–0.1Ti alloy. During cooling the structure factor was monitored by neutron diffraction in time steps of 1 min. During the liquid to solid phase transformation the liquid peaks in the structure factor (Fig. 1) gradually decrease while the Bragg peaks from the solid phase emerge and grow. As the observed Bragg peak intensity strongly depends on texture in the solid phase, we use the scattering from the liquid phase to determine the liquid and solid volume fractions.

Figs. 2 and 3 show the behavior of the liquid volume fraction for the Al–0.15TiB_2 and Al–0.1Ti alloys as a function of temperature for different cooling rates, as determined from the normalized variation in the first maximum of the liquid peak in the structure factor, $S(Q)$, at $Q = 2.68$ Å^{-1}. In Table 1 a summary of the experimental transformation temperatures

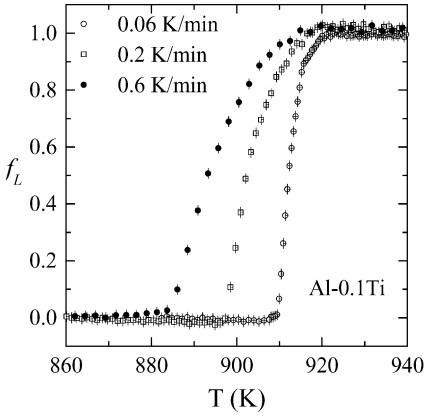

Fig. 3. Liquid volume fraction f_L of the Al–0.1Ti alloy as a function of temperature for cooling rates of 0.06 K/min (open circles), 0.2 K/min (open squares) and 0.6 K/min (solid circles). The liquid volume fraction f_L is deduced from the normalized variation in the first liquid peak in $S(Q)$ at $Q = 2.68$ Å^{-1}.

Table 1
Transformation temperatures of the Al–0.15TiB_2 and the Al–0.1Ti alloys at different cooling rates, where T_s is the transformation start temperature, T_f the transformation finish temperature, and $T_{1/2}$ the temperature for 50% transformation

Sample	Cooling rate (K/min)	T_s (K)	T_f (K)	$T_{1/2}$ (K)	ΔT (K)	$T_0 - T_{1/2}$ (K)
Al–0.15TiB_2	0.06	923	915	918	8	15
	0.60	919	895	906	24	27
Al–0.1Ti	0.06	923	910	912	13	21
	0.20	920	898	902	22	31
	0.60	915	884	893	31	40

In addition, the temperature width of the transformation $\Delta T = T_s - T_f$ and the average undercooling $T_0 - T_{1/2}$ with respect to the crystallization temperature of $T_0 = 933$ K are listed.

as a function of cooling rate is given for both samples. The values mentioned in Table 1 should not be taken as true transition temperatures. As mentioned in the schematic experimental setup [9], the platinum resistance thermometer is placed inside the cylindrical vanadium heating foil. At high temperatures the weak thermal contact between the sample and the liquid metal and a possible inductive coupling between the magnetatic stray fields from the vanadium heating element and the platinum resistance thermometer may cause a temperature shift in the readoub. The real onset temperatures of the transformation should therefore show no significant undercooling as was confirmed in differential thermal analysis (DTA) experiments on smaller samples for low cooling rates. However, once the transformation starts the temperature width of the transformation, shown in Figs. 2 and 3, closely represent that for the sample under study. These results indicate that for the same cooling rate the transformation extends over a wider temperature range in the Al–0.1Ti alloy compared to that of the Al–0.15TiB_2 alloy. The temperature where half of the liquid volume of the Al–0.15TiB_2 and Al–0.1Ti alloys is transformed to solid ($T_{1/2}$) decreases by 12 and 19 K, respectively, for a 10-fold increase in cooling rate. Compared to the pure aluminum sample [9], the liquid/solid phase transformation of both the Al–0.15TiB_2 and the Al–0.1Ti alloys occurs over a wider temperature range irrespective of the cooling rate.

As expected for a phase transformation that involves latent heat, the melting/freezing transition exhibits thermal hysteresis [14]. In Figs. 4 and 5 this thermal hysteresis is shown for combined heating and cooling experiments on Al–0.15TiB_2 and Al–0.1Ti alloys for a heating/cooling rate of 0.6 K/min. The thermal hysteresis of the transformation temperature for 50% the transformation is $\Delta T_{1/2} = 33.6$ K for both samples. The corresponding hysteresis expressed in time is $\Delta t_{1/2} = 56$ min. The observed thermal hysteresis is far too large to be caused by a weak thermal link between the sample and the thermometer, as for our sample with furnace insert [9] the estimated response time for thermal equilibrium is about 5 min, giving rise to a thermal hysteresis of about 10 min during heating/cooling cycle, which is significantly lower than the observed thermal hysteresis in the samples.

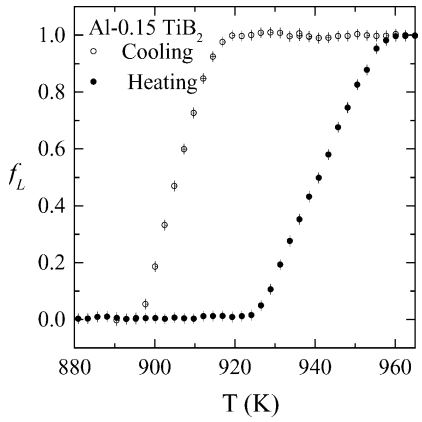

Fig. 4. Liquid volume fraction f_L of the Al–0.15TiB_2 alloy as a function of temperature for cooling (open circles) and heating (solid circles) at a cooling rate of 0.6 K/min. The liquid volume fraction f_L is deduced from the normalized variation in the first liquid peak in $S(Q)$ at $Q = 2.68$ Å^{-1}.

3.3. Transformation kinetics

The crystallization kinetics during isothermal phase transformations has been widely studied using the Johnson–Mehl–Avrami (JMA) model [15-18], with examples in glasses [19,20], gels [21,22], polymers [23], steels [24], and metal alloys [25,26]. According to this model the crystallized fraction, f, can be described as a function of time, t, by the following equation:

$$f(t) = 1 - \exp\{-k(t - t_0)^n\}, \quad (1)$$

where k is the rate constant, t_0 the incubation time, and n the Avrami exponent. The value of the exponent, n, is expected to vary between 1 and 4 depending on the nucleation mechanism and the growth dimensionality [27]. For our continuous cooling experiments the time-dependent undercooling and the release of latent heat during the transformation can lead to a complicated variation in local temperature as a function of time. As a consequence, the growth rate may show a significant time dependence. Given these limitations we feel that the application of the JMA model can give qualitative information on (1) the nucleation process and (2) the relative growth rates. For continuous cooling the transformation time, t, in the JMA equation can be set to zero at the time the temperature falls below the crystallization temperature, T_0 = 933 K [9,23]. Under the assumption that the transformation kinetics depends on the transformation time and is independent of temperature, one can fit the experimental data to the JMA model of Eq. (1). Provided that there is no change in the nucleation and growth mechanisms during the phase transformation, the Avrami exponent, n, is expected to be constant [28] and was found to be $n \approx 3$ for the liquid to solid phase transformation in pure aluminum and in the Al–0.3Ti–0.02B alloy for cooling rates of 0.6 and 0.06 K/min [9].

In Figs. 6 and 7 the solid volume fraction, $f_S(t) = 1 - f_L(t)$, deduced from the liquid fraction is shown as a function of time for the Al–0.15TiB_2 and Al–0.1Ti alloys for cooling rates of 0.06 and 0.6 K/min. The results of a fit of the JMA equation for fixed values of n and t_0 to the experimental data are listed in Table 2, which effectively probes the combined

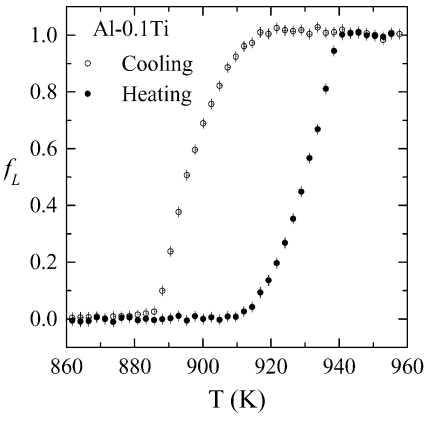

Fig. 5. Liquid volume fraction f_L of the Al–0.1Ti alloy as a function of temperature for cooling (open circles) and heating (solid circles) at a cooling rate of 0.6 K/min. The liquid volume fraction f_L is deduced from the normalized variation in the first liquid peak in $S(Q)$ at $Q = 2.68$ Å^{-1}.

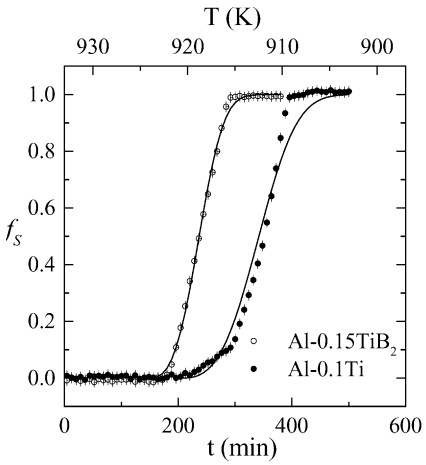

Fig. 6. Evolution of the solid volume fraction $f_S = 1 - f_L$ for the Al–0.15TiB_2 (open circles) and the Al–0.1Ti alloy (solid circles) at a cooling rate of 0.06 K/min. The solid line shows a fit to the data with the Johnson–Mehl–Avrami model (see text).

Table 2
Transformation parameters of the Al–0.15TiB_2 and the Al–0.1Ti alloys at different cooling rates obtained from a fit of the experimental solid volume fraction to the JMA model, where n is the Avrami exponent, k is the rate constant, t_0 is the transformation start time, and $t_{1/2} - t_0 = [\ln(2)/k]^{1/n}$ is the time for 50% transformation after the start of the transformation

Sample	Cooling rate (K/min)	n	k (min^{-n})	t_0 (min)	$t_{1/2} - t_0$ (min)
Al–0.15TiB_2	0.06	3.1	$9.4(3) \times 10^{-7}$	160	75.3
	0.60	3.1	$2.0(7) \times 10^{-5}$	22	28.3
Al–0.1Ti	0.06	3.1	$1.4(7) \times 10^{-7}$	200	138
	0.20	3.1	$8.1(4) \times 10^{-7}$	70	79
	0.60	3.1	$8.4(3) \times 10^{-6}$	30	37.3

The time when the temperature falls below the crystallization temperature T_0 = 933 K is chosen as t = 0.

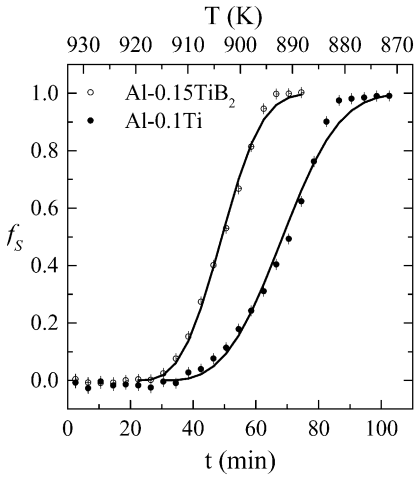

Fig. 7. Evolution of the solid volume fraction $f_S = 1 - f_L$ for the Al–0.15TiB_2 (open circles) and the Al–0.1Ti alloy (solid circles) at a cooling rate of 0.6 K/min. The solid line shows a fit to the data with the Johnson–Mehl–Avrami model (see text).

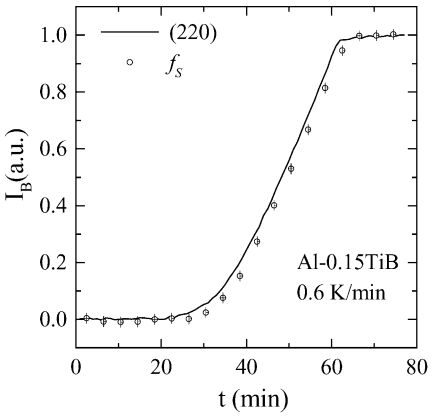

Fig. 8. Normalized integrated Bragg peak intensity I_B for the (2 2 0) reflection of the Al–0.15TiB_2 alloy as a function of the time t for a cooling rate of 0.6 K/min. For comparison the evolution of the solid volume fraction $f_S = 1 - f_L$ deduced from the variation in the first liquid peak in $S(Q)$ is shown.

effect of the grain density and the average growth rate. The corresponding fitted curves are shown in Figs. 6 and 7. The results indicate that the rate constant, k, of the Al–0.1Ti alloy is an order of magnitude lower than that of the Al–0.15TiB_2 alloy. The fully solidified Al–0.15TiB_2 and Al–0.1Ti samples were also investigated using light microscopy. A relatively large grain size was observed for both samples indicating the absence of a significant grain refinement. The variation in the rate constant k for these samples reflects a difference in the average growth rate caused by the solute titanium in Al–0.1Ti alloy rather than by a difference in nucleated grain density. By increasing the cooling rate, the rate constant k increases for both samples. The variation in rate constant for different cooling rates suggests that the average growth rate is enhanced for higher cooling rates due the larger value of the maximum undercooling during the slow transformations under (quasi) equilibrium conditions. The values of rate constant for the Al–0.15TiB_2 alloy at cooling rates of 0.06 and 0.6 K/min are close to those observed for pure aluminum [9] indicating that the TiB_2 particles in pure aluminum do not significantly change its transformation kinetics during solidification. Our observations are in agreement with the results reported by Mohanty et al. [29,30] for the grain refinement process of aluminum in the presence of TiB_2 particles with a diameter about 5 μm and at various solute titanium concentrations. In the absence of solute titanium, no grain refinement was observed. Thus, the results obtained from the present neutron diffraction measurements support the theory that TiB_2 particles in pure aluminum are not effective nucleation sites for the α-Al grains during solidification. The observed value of $t_{1/2}$ for the Al–0.15TiB_2 alloy is lower than that of the Al–0.1Ti alloy for both cooling rates, confirming the relatively slow crystallization during the solidification of the Al–0.1Ti alloy.

3.4. Intensity fluctuations

Fig. 8 shows the evolution of the solid fraction and the corresponding Bragg peak intensity from the (2 2 0) reflection of the α-Al (f.c.c.) grains in the Al–0.15TiB_2 alloy during solidification with a cooling rate of 0.6 K/min. The observed liquid to solid phase transformation is continuous and no anomalous behavior is observed. However, during the early stages of the liquid to solid phase transformation of the Al–0.1Ti alloy, the variations in the Bragg peak intensity from the nucleating crystallites were observed. These variations in Bragg peak intensity are present in all the observed Bragg reflections and for different cooling rates. Fig. 9 shows the evolution of the (3 1 1) Bragg reflection in the Al–0.1Ti alloy for cooling rates of 0.06, 0.2 and 0.6 K/min. The observed behavior is quite similar to that of previously reported results for the solidification of the Al–0.3Ti–0.02B alloy [9,31]. However, for the solidification of the Al–0.3Ti–0.02B alloy, these time-dependent Bragg peak intensity fluctuations were present during the whole liquid to solid phase transformation process. For the Al–0.1Ti alloy the intensity fluctuations were only observed during the early stage of the solidification process (for $f_S < 0.20$) at all cooling rates. When the solidification is complete, a change in Bragg peak intensity is observed, which is probably due to coarsening of the solid grains at high temperature.

The observed fluctuations in Bragg peak intensity at the beginning of the solidification process in the Al–0.1Ti alloy, limits our ability to analyze the possible dynamics of phase transformation during solidification. These fluctuations in Bragg peak intensity are probable due to the motion of few individual crystallites that are formed at the start of the solidification process. Easton and StJohn [2] proposed that at the beginning of solidification the driving force for nucleation is usually thermal undercooling in the melt at the sample container wall and then the titanium partitioning between the solid-liquid interface leads to constitutional undercool-

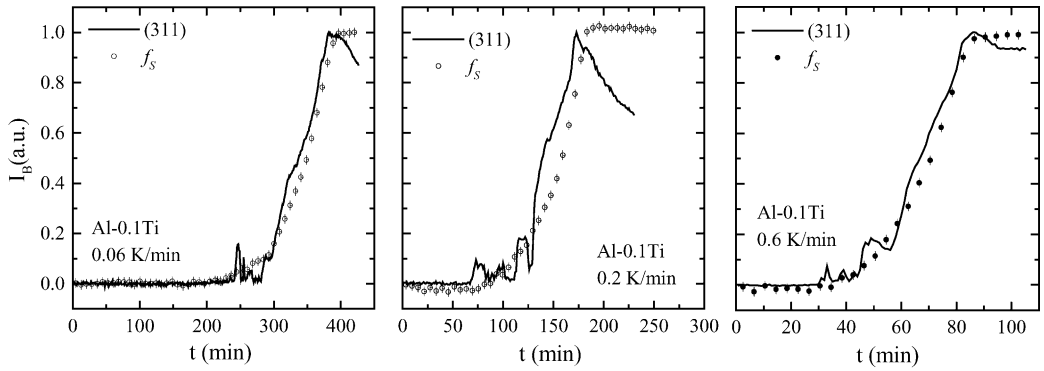

Fig. 9. Normalized integrated Bragg peak intensity I_B for the (3 1 1) reflection of the Al–0.1Ti alloy as a function of the time t for a cooling rate of 0.06, 0.2 and 0.6 K/min. For comparison the evolution of the solid volume fraction $f_S = 1 - f_L$, deduced from the variation in the first liquid peak in $S(Q)$, is shown.

ing immediately ahead of the growing solid, in which the nucleant particles become activated for nucleation. In such a case the grains produced during the early crystallization process in the Al–0.1Ti alloy will be bound to the container surface and their motion is not probable. Therefore it appears that in the beginning of the solidification of the Al–0.1Ti alloy, nucleation starts in the liquid aluminum, away from the container wall. This is possible only if there exist some effective nucleation sites inside the melt. As no impurity particles are expected in the Al–0.1Ti alloy because of the high purity of the starting materials used, it is probable, as predicted by the duplex nucleation theory [29], that the formation of $TiAl_3$ takes place even at concentrations of titanium below the peritectic composition of < 0.15 wt.% Ti. Since $TiAl_3$ is an effective nucleation site for α-Al grains, it can activate the crystallization process in the aluminum melt, away from the container wall and the motion of these crystallites can give rise to the observed intensity fluctuations. This observation supports the hypothesis that when both TiB_2 particles and solute titanium is present in liquid aluminum, even at the hypoperitectic composition, a layer of $TiAl_3$ coats TiB_2 particles, thus making it an effective nucleation site during the grain refinement process in aluminum and is needed for epitaxial growth of nucleating grains of aluminum. However, further investigations are necessary to validate this theory.

4. Conclusions

This paper presents the structural and kinetic features of the crystallization kinetics in Al–0.15TiB_2 and Al–0.1Ti alloys as a function of cooling rate during continuous cooling. The results obtained from these measurements support the theory that TiB_2 particles in pure aluminum are not effective nucleation sites for the α-Al grains in liquid aluminum during solidification. The presence of solute titanium in aluminum causes a significant change in the growth kinetics. The crystallization behavior of the Al–0.1Ti alloy indicates the possible formation of a $TiAl_3$ phase responsible for the nucleation of aluminum grains.

Acknowledgements

We gratefully acknowledge the technical assistance by Y.K. Huang from the University of Amsterdam for the preparation of the Al–1Ti master alloys. Thanks are due to the Institute Laue-Langevin for the beam time provided to perform the neutron diffraction experiments. This work was financed in part by the Netherlands Foundation for Fundamental Research of Matter (FOM) and the Netherlands Institute for Metals Research (NIMR).

References

[1] M. Easton, D. StJohn, Met. Mater. Trans. A 30 (1999) 1613.
[2] M. Easton, D. StJohn, Met. Mater. Trans. A 30 (1999) 1625.
[3] A. Cibula, J. Inst. Met. 80 (1951) 1.
[4] A. Marcantonio, L.F. Mondolfo, Metal. Trans. 2 (1971) 465.
[5] I. Maxwell, A. Hellawell, Acta Metal. 23 (1974) 229.
[6] L. Backerud, Light Metal Age 41 (1983) 6.
[7] G.K. Sigworth, Metal. Trans. A15 (1984) 277.
[8] A.L. Greer, A.M. Bunn, A. Tronche, P.V. Evans, D.J. Bristow, Acta Mater. 48 (2000) 2823.
[9] N. Iqbal, N.H. van Dijk, V.W.J. Verhoeven, W. Montfrooij, T. Hansen, L. Katgerman, G.J. Kearley, Acta Mater. 51 (2003) 4497.
[10] S. Takeda, Y. Kawakita, M. Inu, K. Maruyama, S. Tamaki, Y. Waseda, J. Non-Cryst. Solids 205–207 (1996) 365.
[11] S. Takeda, S. Harada, S. Tamaki, Y. Waseda, J. Phys. Soc. Jpn. 60 (1991) 2241.
[12] Y. Waseda, The Structure of Non-Crystalline Materials, McGraw-Hill, New York, 1980.
[13] IAMP database of SCM-LIQ, Tohoku University. URL: http://www.iamp.tohoku.ac.jp/database/scm/LIQ/sq.html.
[14] A.B. Herhold, H.E. King, E.B. Sirota, J. Chem. Phys. 116 (2002) 9036.
[15] J. Johnson, R. Mehl, Trans. AIME 135 (1939) 416.
[16] M. Avrami, J. Chem. Phys. 7 (1939) 1103.
[17] M. Avrami, J. Chem. Phys. 8 (1940) 212.
[18] M. Avrami, J. Chem. Phys. 9 (1941) 177.
[19] Y.M. Sung, S. Kim, J. Mater. Sci. 35 (2000) 4293.
[20] A.F. Gualtieri, E. Mazzucato, C.C. Tang, R.J. Cernik, Mater. Sci. Forum 312 (2000) 224.
[21] A.M. Fogg, S.J. Price, J.J. Francis, S. O'Brien, D. O'Hare, J. Mater. Chem. 10 (2000) 2355.
[22] J. Malek, Thermochem. Acta 355 (2000) 239.

[23] P. Supaphol, J. Appl. Pol. Sci. 78 (2000) 338.
[24] D.V. Louzguine, A. Inoue, J. Mater. Sci. 35 (2000) 4159.
[25] J.K. Lee, G. Choi, D.H. Kim, W.T. Kim, Appl. Phys. Lett. 77 (2000) 978.
[26] C.A.C. Imbert, H. MacQueen, J. Mater. Sci. Technol. 16 (2000) 532.
[27] D.W. Henderson, J. Thermal. Anal. 15 (1979) 325.
[28] D.A. Porter, K.E. Easterling, Phase Transformations in Metals and Alloys, Chapman & Hall, London, 1993.
[29] P.S. Mohanty, J.E. Gruzleski, Acta. Metall. Mater. 43 (1995) 2001.
[30] P.S. Mohanty, F.H. Samuel, J.E. Gruzleski, Metall. Mater. Trans. 26B (1995) 103.
[31] N. Iqbal, N.H. van Dijk, V.W.J. Verhoeven, T. Hansen, L. Katgerman, G.J. Kearley, Mater. Sci. Eng. A 367 (2004) 82.